Method for calculating the urea release and decomposition in the NOxOUT process in the context of a live optimization approach

D. Beerbaum[1], D. Bernhardt[1], T. Jakobs[2], M. Beckmann[1], T. Kolb[2]
daniel.beerbaum@tu-dresden.de
[1]EVT, TU Dresden, Germany
[2]ITC, Karlsruhe Institute of Technology, Germany

Abstract

The motivation for this work is the development of a live optimization tool to control the additive input of the selective non-catalytic reduction (SNCR) process. An essential component of the model is the description of the additive input by technical spray nozzles. This approach aims to provide sufficiently accurate results through targeted simplifications with short computation times. Established CFD calculation methods do not meet this requirement.
Based on an already developed semi-analytical approach to calculate the mass transfer of technical sprays into a reaction environment [1], this paper demonstrates the feasibility of a future potential implementation via comparison with a CFD study. In preparation for a practical application, the evolution of the existing model to consider urea injection and decomposition under typical SNCR conditions is also presented. Initially, the drying and formation of a solid urea crust is considered. Followed by complete particle drying, the release occurs due to the thermal decomposition of the urea. Part of the assumptions made based on experimental studies of single droplet evaporation of urea-water solutions (UWS) in an ultrasonic levitator.
The extension of the model to include the reaction kinetics of the subsequent Nitrogen oxide (NO) reduction reactions is still to do at this point.

Introduction

The SNCR process is an important tool for the cleaning of flue gases, especially for small plants such as biomass and waste furnaces. For nitrogen oxide reduction, ammonia (NH_3), urea (CN_3H_4O) or isocyanic acid ($HNCO$) is sprayed into the hot flue gas via cooled lances. Technical innovations can be found in the areas of temperature monitoring [2, 3], nozzle positioning [4] and additive addition [5], as well as the use of numerical CFD calculations to design or optimize the process [6, 7].
Changes in the composition of the flue gas due to permanently changing fuel composition (waste incineration plant) as well as the specific distribution of the pollutants over the boiler cross-section (grate firing) have so far been neglected in the control of SNCR plants. The inclusion of these operating parameters has the potential for a more targeted operation of the SNCR, which would reduce the NH_3 slip and save additive quantities.
In addition to knowledge of the fuel composition [8] and the resulting NO distribution [9] a fast computational approach to determine the optimal additive distribution is needed for live optimization of SNCR.
An already developed semi-analytical model approach for the determination of the mass transfer from technical spray nozzles [1] s tested for this purpose in a comparative observation with a CFD study. Based on this, a further development of the approach for the consideration of the use of urea in the NOxOUT process [10] has taken place.

Brief Summary of the fundamental Model approach

The initial point of the model is the linked description of the droplet evaporation with the droplet movement. This provides a differential equation system whose solution defines the spatial and temporal distribution of the evaporated spray medium in a reaction chamber. [2]
The approach to droplet motion is a description of the droplet path via the equilibrium of the forces acting on the droplet. Gravitational, buoyant and aerodynamic forces are taken into account, as well as the force effect of a flow of the surrounding gas phase. The solution of the resulting differential equation (equation 1) provides the time-dependent location and velocity of the drop.
The basis for the development of the evaporation models is the description of the single droplet evaporation by the well-known D² law (equation 2). The D² law assumes a limitation of the evaporation rate by the heat transport in the droplets and a limitation by the mass transport from the phase boundary into the environment [11, pp. 399 - 406]. This approach been further developed during model evolution and supplemented by additional theories [12, 13, 14, 15] The resulting model approach (equation 3 - 7) takes into account a velocity difference between the droplet and the gas phase, as well as the sensible heating of the liquid.

$$\frac{\partial^2 \vec{x}}{\partial t^2} = \frac{1}{m_D} \sum \vec{F}_i \tag{1}$$

$$(2 \cdot r_D(t))^2 = (2 \cdot r_0)^2 - 8 \cdot a_v \cdot \frac{\rho_v}{\rho_l} \cdot ln\left(1 + \frac{c_{p,l}(T_\infty - T_0)}{\Delta h_{ev}}\right) \cdot t \tag{2}$$

$$\frac{dm}{dt} = 4 \cdot \pi \cdot r(t) \cdot \rho_{film} \cdot D_{BA} \cdot \ln(1 + B_M) \left(1 + \frac{0{,}552 \cdot \sqrt{2}}{2} \frac{Sc^{\frac{1}{3}} \left(\frac{Re}{2}\right)^{\frac{1}{2}}}{(1 + B_M)^{0{,}7} \cdot \frac{\ln(1 + B_M)}{B_M}}\right) \tag{3}$$

with

$$B_M = \frac{\xi_{B,S} - \xi_{B,\infty}}{1 - \xi_{B,S}}; \tag{4}$$

$$Re = \frac{2 \cdot r_{cs}(t) \cdot \left|\frac{d\vec{x}}{dt} - \vec{U}_\infty\right|}{\nu}; \tag{5}$$

$$Sc = \frac{\nu_{film}}{D_{BA}} \tag{6}$$

The drop radius is determined as:

$$\frac{dr}{dt} = \frac{1}{4 \cdot \pi \cdot \rho_{H2O} \cdot r^2} \cdot \frac{dm}{dt} \tag{7}$$

To validate the formulated model approaches, experimental investigations of single-droplet evaporation carried out on an ultrasonic levitator. For this purpose, a single droplet is held in a resting floating position via a standing resonance wave (see figure 1), so that the investigation of complete evaporation is possible. A special feature here is the minimization of possible interfering influences.

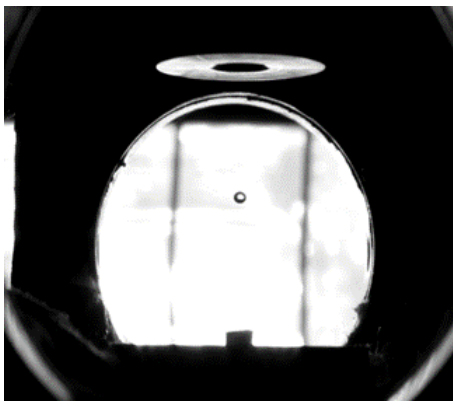

Figure 1: Floating drop in the levitator

Figure 2 shows a top view of the measurement setup at the four openings of the levitator. A temperature-controlled heating cartridge with air flowing through it heats the near ambient air at the levitating droplet. Another reference temperature measured behind the drop. The evaporation of the drop recorded with a high-speed (HS) camera. The decrease of the droplet diameter over the evaporation time is determined by analyzing the recorded image material.

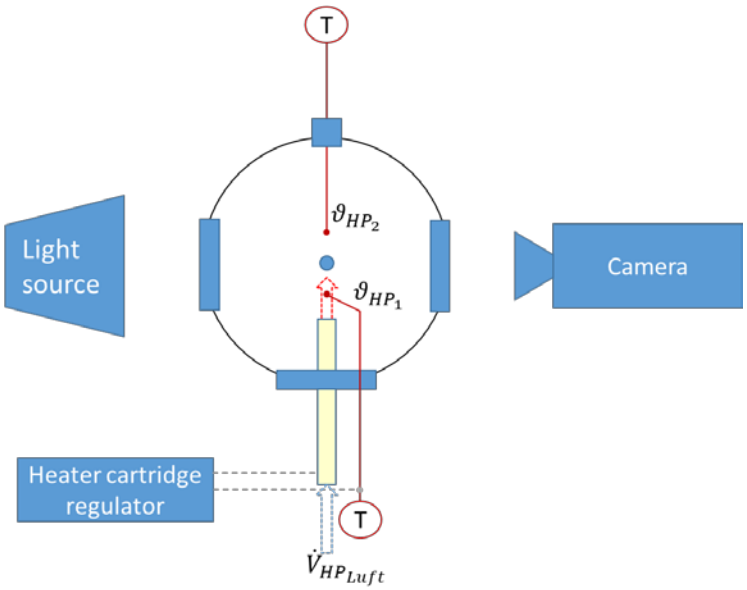

Figure 2: Measurement setup on the Levitator (top view)

Comparative view with a CFX studie

For a first application test, results of the complete simplified spray model compared with a simplified non-validated CFX calculation of a SNCR injection. This comparative observation therefore does not represent a validation of the model, but rather shows the applicability of the model by providing an example.

The injection of water via four spray nozzles into a boiler pass with vertical flue gas flow is calculated. Initial data such as velocities, temperatures, geometric dimensions and nozzle characteristics taken from the CFX calculation.

Figure 3 shows the influence of the nozzle characteristics on the calculation. The simplified description of the nozzle characteristic via an RRSB distribution (data from CFX calculation) compared here with the radially distributed characteristic of the same nozzle determined by measurement. The reaction chamber divided into 10x10x10 volume elements. A colored sphere in the plots represents the volume elements with portions of the evaporated spray medium. The coloring provides information about the normalized proportion of the evaporated fluid mass. When analyzing the graphs, it must taken into account that the color scale is logarithmic. In both calculation cases, the main part of the spray medium is evaporated in the volume element located downstream of the nozzle. Subsequently, the discharge takes place with the flue gas flow in the Z-direction. The much broader and deeper distribution in the

calculation case with the measured data is due to small proportions of large droplets in the size distribution of the spray. These penetrate deeper into the reaction chamber.

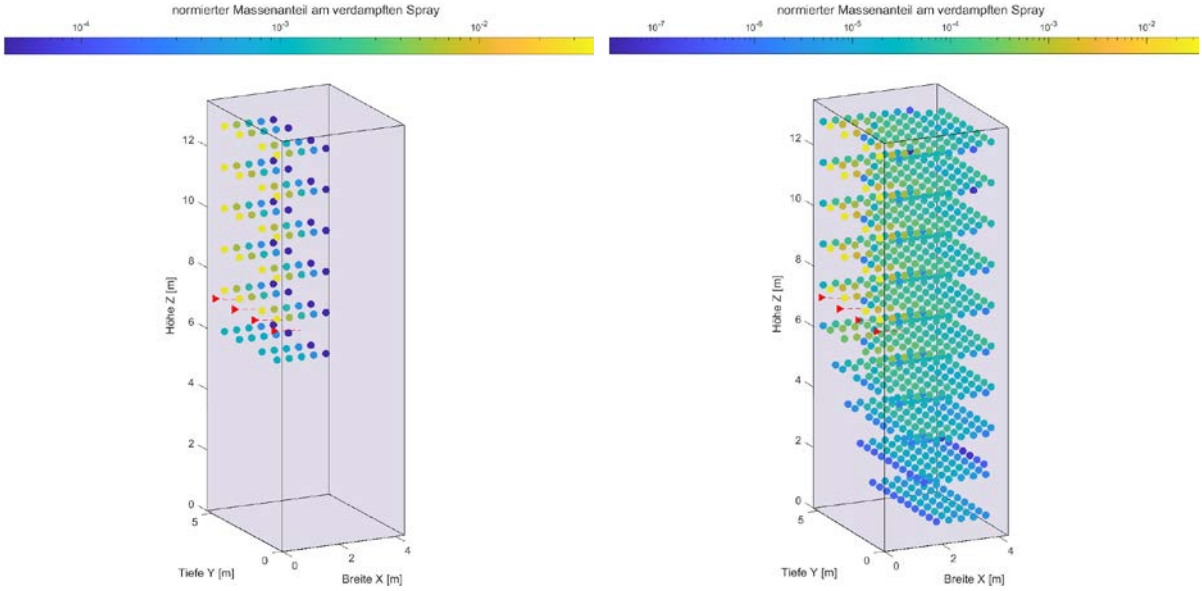

Modell calculation with nozzle data from CFX input

Modell calculation with measured nozzle data

Figure 3: Comparison of the calculation of an SNCR injection for different nozzle data

The comparison of the calculation results of the simplified model and the CFX calculation shows similarities in the global view. For example, the total amount of spray medium temporarily present in the reaction space is the same in both calculations. In addition, the expansion of the spray over the height is the identical in both calculations (see figure 4).
In the more detailed examination of figure 4, deviations in the model results become clear. Figure shows relatively constant distribution of the mass of evaporated water over height from nozzle level for both spray characteristics while the CFX calculation shows an increase with increasing height. One reason for this may be the early beginning of the outlet, which leads to a redirection of the flue gas flow. The simplified model neglects this deflection of the flue gas flow.

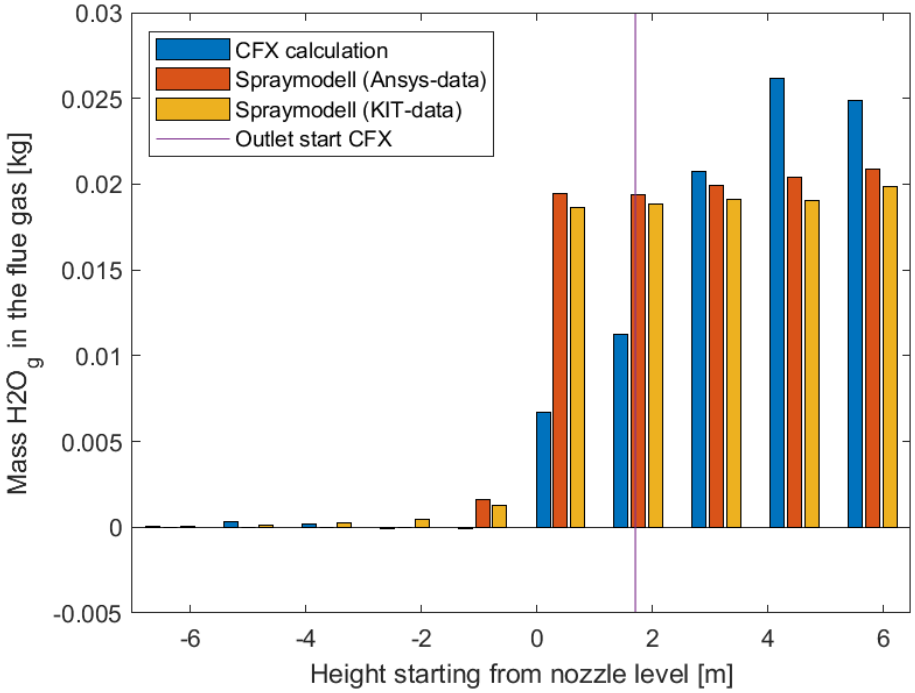

Figure 4: Water mass fraction in flue gas versus height

In a further observation, the resulting distribution of the evaporated water mass in the spray plane of both models was compared. For better comparability, the mass fraction for 10 x 10 representative volume elements was generated from the results of the CFX calculation (see figure 5). With a subsequent adjustment of the color scale, a direct comparison of the results is now possible (see figure 6). The figure shows that discrepancies arise also with this more detailed observation. In the simplified model, as can already be seen in figure 3, the main part of the droplet mass evaporates in the volume element after the nozzle. The physical explanation for this is that the droplets are largest here and thus offer the largest area of transmission. In addition, the largest velocity difference between droplet and gas phase is located here, which is also a critical variable for droplet evaporation [3]. Furthermore, a symmetry of the individual nozzles can see in the simplified model. In the result of the CFX calculation, the distribution of the evaporated water is asymmetrical. The maxima here are located at a greater distance from the nozzles and are not as distinct as in the simplified model. Overall, there is a broader distribution of the evaporated medium in the plane. A main cause for this distribution is horizontal flow components from the vortexing of the flue gas. This detailed modeling of the flue gas flow not implemented in the simplified model.

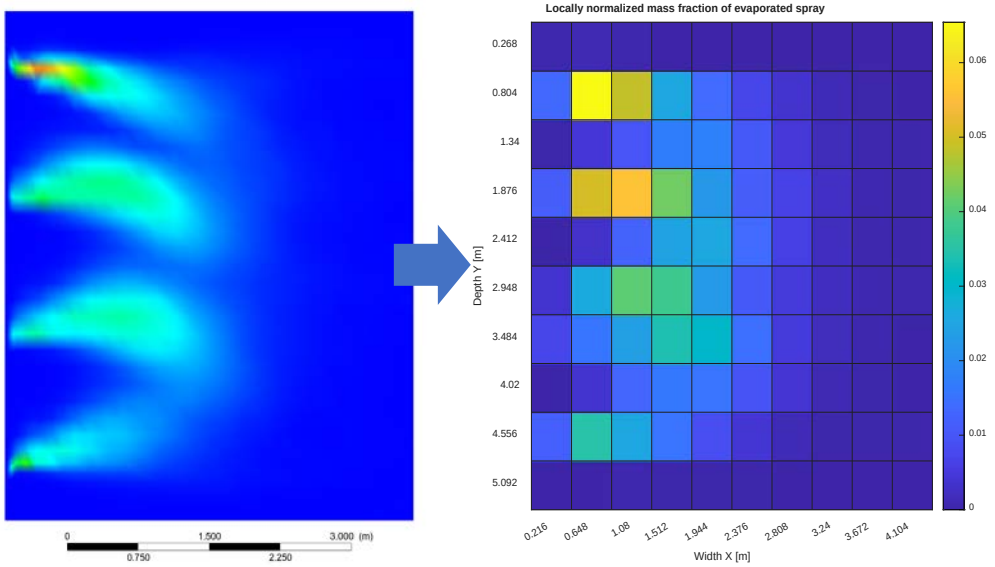

Figure 5: Transformation of the local water mass distribution (spray nozzle level) from CFX calculation into a 10 x 10 structure

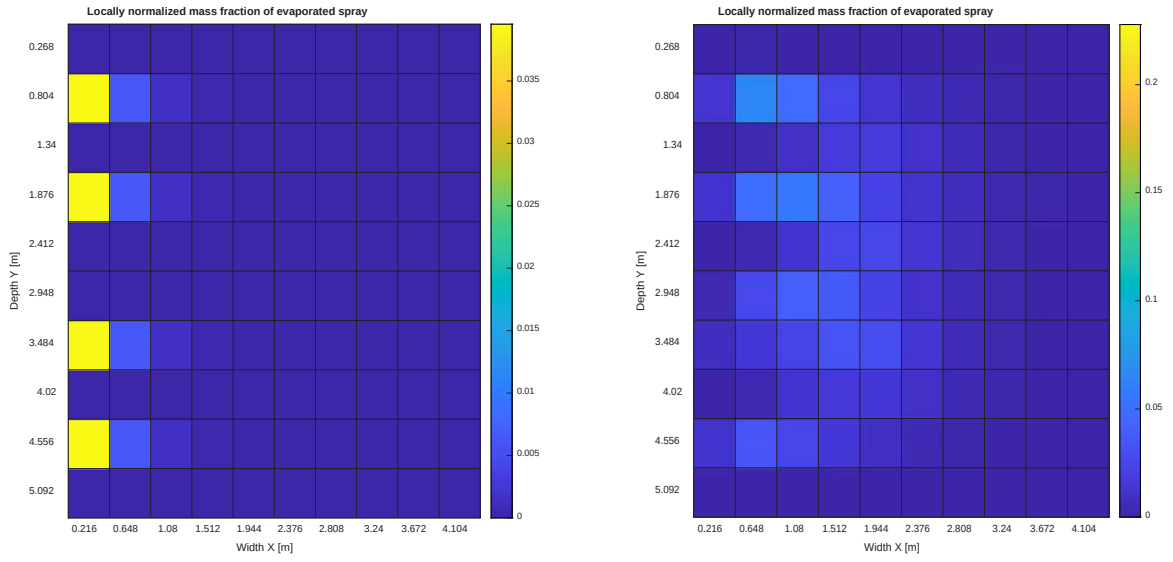

Figure 6: Comparison of the distribution of evaporated water at the spray nozzle level (on the left: simplified model, on the right: CFX calculation)

Evaporation and Thermolysis of Urea

In the following, the boundary conditions of the substance input will examined for SNCR operation with urea. The injected UWS has a urea mass fraction in a range of $40 - 45\ \%$. The temperature window for SNCR operation with urea is in the range $850\ -\ 950\ °C$. [16]
The following specific properties of urea considered for the extended model approach:

- Urea has a high solubility in water. [17]
- The vapor pressure of urea is significantly lower than that of water. [18]
- The melting point of urea is 133 °C. [18]
- In the course of evaporation of urea CN_3H_4Oit thermally decomposes to NH_3 and $HNCO$: [19]

$$CN_3H_4O \rightarrow NH_3\ +\ HNCO$$
$$\Delta h_{decomp} = 3088{,}8\ \frac{\mathrm{kJ}}{\mathrm{kg}} \tag{8}$$

The exact decay conditions are not completely known. In the literature, various data can found, e.g. on the decomposition temperature. [20]
In a recent work, Bernhardt et. al. showed that urea can to a large extent change into the gas phase at temperatures up to $153\ °C$. [21]. In the present work, the thermal decomposition of urea is considered from a temperature of $152\ °C$ or $425\ K$ according to Schaber et. al. [22].
For further consideration, temperature and concentration changes in the droplet are neglected in the sense of a rapid mixing model approach. Furthermore, the droplets are described by a spherical geometry. For the determination of temperature and substance values at the phase boundary, the established 1/3 rule of Hubbard et. al. is applied: [23]

$$T_{film} = T_D + \frac{1}{3}(T_\infty - T_D) \tag{9}$$
$$Y_{film} = Y_{v,S} + \frac{1}{3}(Y_{v,\infty} - Y_{v,S}) \tag{10}$$

To determine the urea release, the description of the evaporation of the UWS divided into three phases:

- Phase I: Pure water evaporation until urea solubility limit is reached
- Phase II: Formation of a urea crust, calculation of crust growth as well as particle drying
- Phase III: Thermal decomposition of the urea crust

Phase I:

First, the drop appears as a drop of pure water. Due to the low vapor pressure of urea, this is permissible to a good approximation. Phase I ends as soon as the solubility limit is reached in the droplet. The calculation of the pure substance evaporation follows based on the already developed model approach (equation 3 - 7).
The evaluation of experimental tests with UWS drops on the ultrasonic levitator show that the approximation of the first evaporation phase with a pure substance model for water is legitimate. The model reproduces the evaporation behavior very well (see figure 7).
For the evaluation of the model description of the following evaporation phases, the experimental methodology is not suitable. This is on the one hand due to the fact that the method records the decrease of the radius. This remains initially constant during crust formation. Moreover, the conditions for urea decomposition cannot currently be set in the experimental setup.

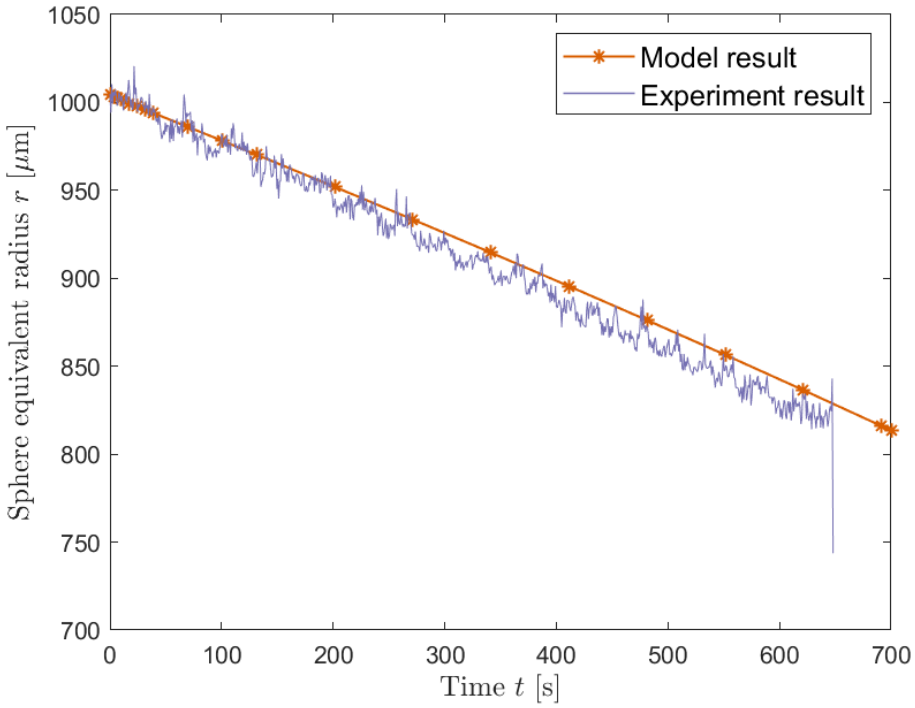

Figure 7: Result comparison of the pure substance model for water with the evaluation of a single drop evaporation experiment in the ultrasonic levitator

$$(\xi_{Urea,0} = 0.33; T_\infty = 300\ K; p_\infty = 1{,}0133\ bar;\ \left|\frac{d\vec{x}}{dt} - \vec{U}_\infty\right| = 0{,}05\frac{m}{s}; \xi_{H2O,\infty} = 0.009; \xi_{Urea,\infty} = 0)$$

Phase II:

After reaching the solubility limit, a solid urea crust forms on the surface of the droplet. Inside is a moist core of aqueous saturated urea solution. The second evaporation stage describes the growth of the crust as well as the drying of the particle. The water evaporates through pores in the crust. A porous, dry crust with a solid surface develops. The wet core – the area where the pores are filled with solution – (figure 8) becomes progressively smaller until the particle is completely dried.

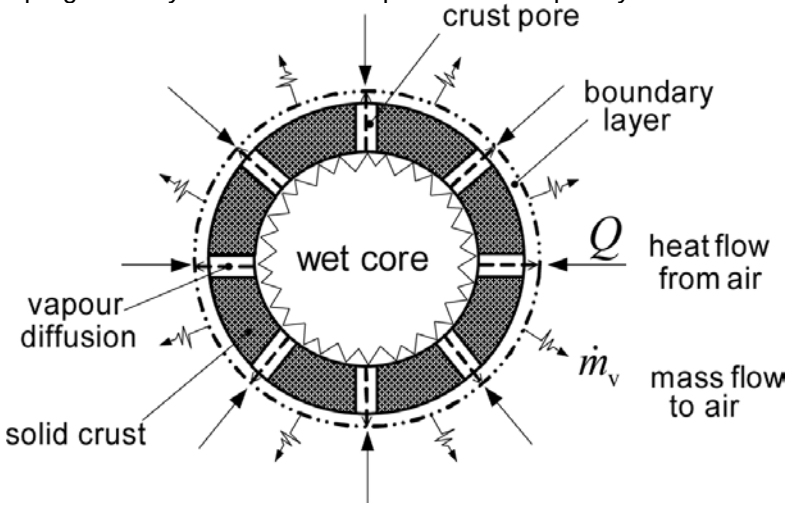

Figure 8: Scheme of wet particle dehumidification **[24]**

In experimental studies using the ultrasonic levitator, the formation of a solid urea crust was observed during the evaporation of a UWS droplet under ambient conditions. Figure 9 shows snapshots of the HS camera image of the crust formation. Figure 10 shows the completely dried urea particle in the levitator.

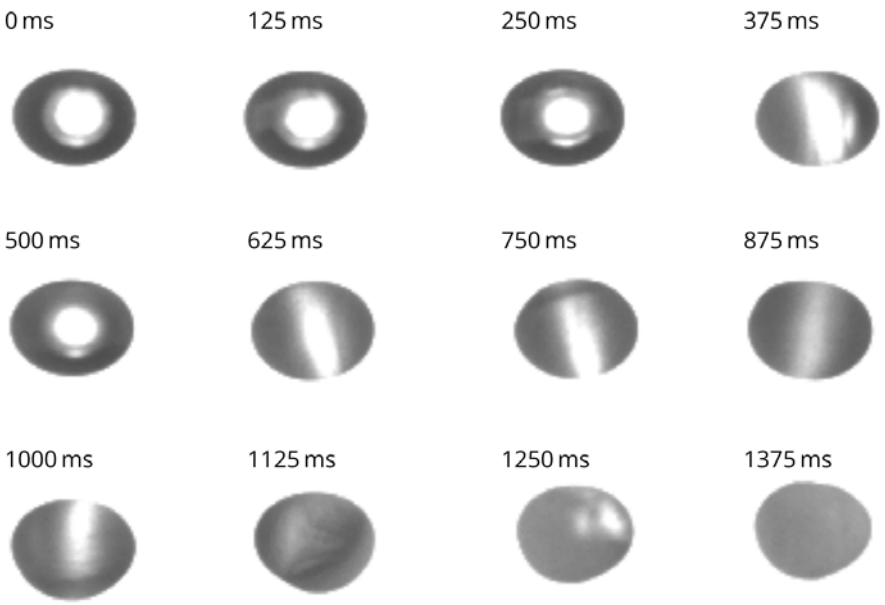

Figure 9: Snapshots of the crust formation of a UWS droplet at ambient atmospheric conditions taken with a high-speed camera

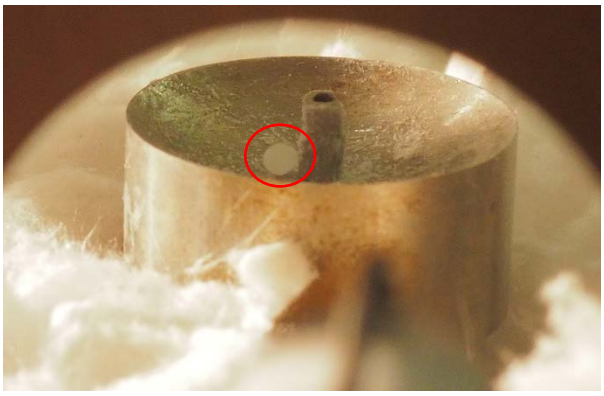

Figure 10: Urea particle resulting from drying in the reflector of the levitator

Phase II describes the crust formation and drying of the urea. The inhibited evaporation of the water takes into account the current crust thickness and the porosity of the urea. The water evaporation cools the urea crust. The melting temperature of the urea is not exceeded. The release of the urea is negligible in this phase. The simplified assumption of complete drying is made.

To describe the evaporation in phase II, a model approach of suspension drying is adapted. In their model approach, Abuaf et. al. represent the porosity of the crust via the simplified concept of pores as straight channels through the crust [25]. Mass transport through the channels is done considering a semi open Stefan's system. A comprehensive review for modeling suspensions and dissolved solids is provided by Mezhericher et. al. [24]. Evaporation with the additional diffusion resistance through the crust is calculated using equation 11.

$$\frac{dm_{H2O,ev}}{dt} = -\frac{4 \cdot \pi \cdot \varepsilon \cdot D_{Gas,H2O} \cdot p_{\infty}}{\mathcal{R}_{H2O}(T_{CS} + T_{WS})} \cdot \frac{r_{CS} \cdot r_{WS}(t)}{r_{CS} - r_{WS}(t)} \cdot \ln\left(\frac{p_{\infty} - p_{H2O,WS}}{p_{\infty} - \left(\frac{\mathcal{R}_{H2O} \cdot \frac{dm_{H2O}}{dt}}{4 \cdot \pi \cdot r_{CS}^2 \cdot B_M} + \frac{p_{H2O,\infty}}{T_{\infty}}\right) \cdot T_{CS}}\right) \tag{11}$$

For the temperature of the wet core T_{WS} it assumes in a good approximation that the established equilibrium temperature from phase I is maintained. The crust surface experiences a temperature increase. This increase can be determined via a simplified energy balance for the crust:

$$\dot{Q}_{conv} = \dot{Q}_{cond} \tag{12}$$

$$\alpha \cdot 4 \cdot \pi \cdot r_{CS}^2 \cdot (T_\infty - T_{CS}(t)) = \frac{4 \cdot \pi \cdot \lambda_{Urea}}{\frac{1}{r_{WS}(t)} - \frac{1}{r_{CS}}} (T_{CS}(t) - T_{WS}) \tag{13}$$

$$T_{CS}(t) = \frac{\alpha \cdot r_{CS}^2 \cdot T_\infty - \frac{\lambda_{Urea}}{\frac{1}{r_{WS}} - \frac{1}{r_{CS}}} \cdot T_{WS}}{\alpha \cdot r_{CS}^2 - \frac{\lambda_{Urea}}{\frac{1}{r_{WS}(t)} - \frac{1}{r_{CS}}}} \tag{14}$$

The temperature increase occurs almost promptly under SNCR conditions (see figure 13). It ends when the melting temperature of the urea arrives. For the temperature of the crust T_{CS} the melting temperature can be used as a good approximation.
The crust radiusr_{CS} corresponds to the drop radius at the end of phase I. The radius of the wet core changes with the evaporated water mass. The relationship can be determined to:

$$\frac{dr_{WS}}{dt} = \frac{1}{4 \cdot \pi \cdot \rho_{H2O} \cdot r_{CS}^2} \cdot \frac{dm_{H2O,ev}}{dt} \tag{15}$$

The dissolved mass fraction in the liquid of the wet core corresponds to the solubility limit. The drying of the particle thus simultaneously determines the crust growth:

$$m_{CR}(t) = m_0 \cdot \xi_{Urea,0} - \left(m_0 \cdot (1 - \xi_{Urea,0}) - m_{H2O,ev}(t)\right) \cdot \frac{\xi_{Urea,max}}{1 - \xi_{Urea,max}} \tag{16}$$

Based on an adaptation of the pure substance model, the evaporation of urea under the conditions mentioned was estimated. In the figure 12, after the crust formation, it can be seen that the urea evaporation is negligible. Especially considering that it gets overestimated by neglecting the evaporating water flow.

Phase III

Phase III describes the release of the urea. It begins as soon as the urea particle is completely dry. The release of the urea occurs by thermal decomposition (equation 17) at $425\,K$. The evaporation of the urea becomes neglect. The description of the thermal decay follows an approach after Ström et. al.: [26]

$$\frac{dm_{Urea,decomp}}{dt} = \frac{\pi \cdot 2 \cdot \lambda_{film} \cdot r_{CS}(t) \cdot Nu}{c_{p_{film}}} \cdot \ln\left[1 + \frac{c_{p_{film}} \cdot (T_\infty - T_{CS})}{\Delta h_{decomp}}\right] \tag{17}$$

The Frössling approach for determining the Nusselt number Nu is applied: [27]

$$Nu = 2 + 0{,}552 \cdot Re^{\frac{1}{2}} Pr^{\frac{1}{3}} \tag{18}$$

For the calculation of the relevant substance data, empirical approaches from the literature [18, 17, 28] were applied, and a commercial substance data add-in for MATLAB [29] was used.

Results and Discussion

The results of the simplified spray model for the exemplary calculation of an SNCR injection show both a global view of the spray input and the local resolution of individual planes. The resolution remains coarser as in the comparable CFX calculation, but significant statements could still made. Compared to the CFX calculation, the simplified model offers the advantage of a much shorter calculation time (10 min with 8 GB RAM, 4 cores versus 14 h with 32 GB RAM, 16 cores). Since both calculation approaches have not yet undergone full validation, only limited conclusions can be drawn about the validity of the results. A major influence on the results of both models is the spray characteristics used. Simplified

assumptions as initial spray data can lead to erroneous results. The strong influence of smoke gas turbulence on the distribution of the spray medium must be taken into account in the future. However, this can only be done based on assumptions, since a three-dimensional flue gas velocity profile in a running boiler plant cannot be measured and is not stationary. Known flow effects such as stranding can certainly take into account in the simplified model.
Based on the successful application test, further development of the simplified model continued. For the description of the NOxOUT process, the material input and thermal decomposition of the additive urea is described by an extension of the known model approach.

The figure 11 - 13 show the result of the described model calculation for the evaporation of a urea water droplet under SNCR conditions. The three model phases can be seen via the marked boundaries of crust formation and urea decay. The mass decrease is initially determined by the evaporation of water. As a result of a minimal heating period, this initially starts slowly and increases to reach the equilibrium temperature at $355{,}5\ K$ (see figure 13). As a result of crust formation, the evaporation rate levels off until complete drying is reached. Urea evaporation in this region is negligible due to the low partial pressure (see figure 12). The crust that forms undergoes a rapid increase until the melting temperature of the urea is reached. After the crust is completely dry, with the absence of evaporative cooling and the melting enthalpy overcome, the crust temperature is assumed to increase rapidly until the urea undergoes thermal decomposition. The mass decrease during the decay is determined by the transferred heat and primarily by the transfer area represented by the instantaneous radius of the crust $r_{CS}(t)$.

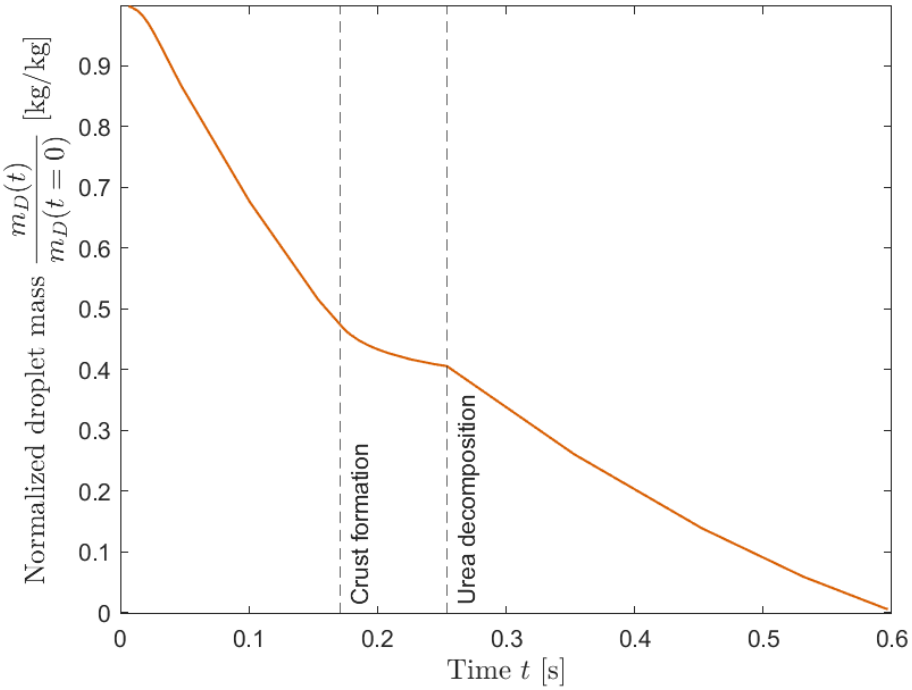

Figure 11: Normalized droplet mass versus time
($r_0 = 200\ \mu m;\ T_\infty = 1223\ K; p_\infty = 1{,}0133\ bar; \xi_{Urea,0} = 0{,}4;\ \left|\frac{d\vec{x}}{dt} - \vec{U}_\infty\right| = 10\frac{m}{s}; \xi_{H2O,\infty} = 0.015;\ \xi_{Urea,\infty} = 0$)

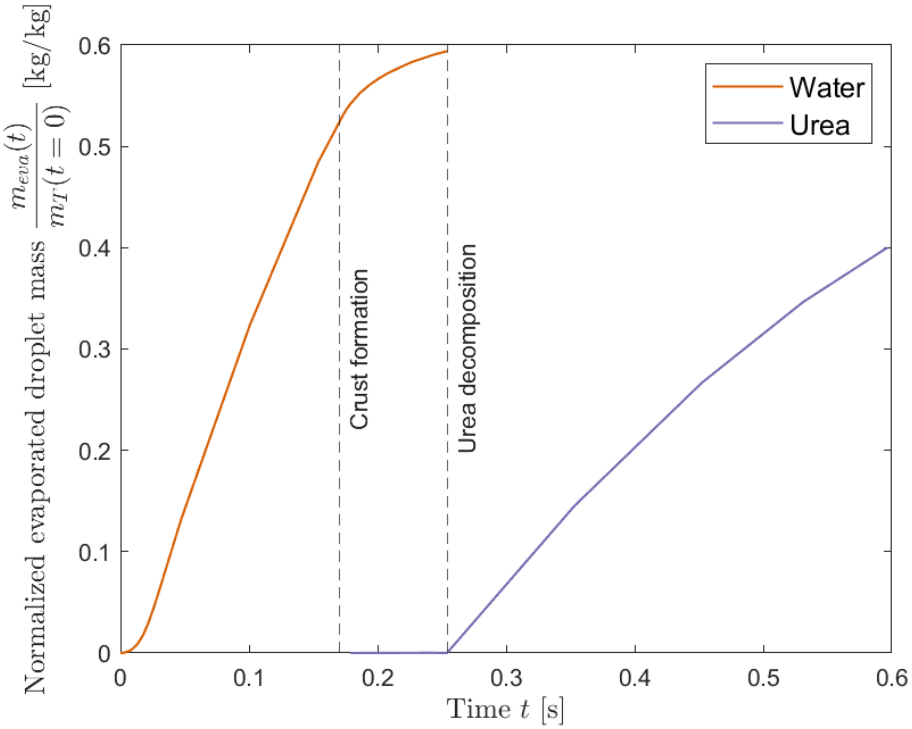

Figure 12: Normalized evaporated droplet mass versus time of water and urea fraction ($r_0 = 200\ \mu m;\ T_\infty = 1223\ K; p_\infty = 1{,}0133\ bar; \xi_{Urea,0} = 0{,}4;\ \left|\frac{d\vec{x}}{dt} - \vec{U}_\infty\right| = 10\frac{m}{s}; \xi_{H2O,\infty} = 0.015;\ \xi_{Urea,\infty} = 0$)

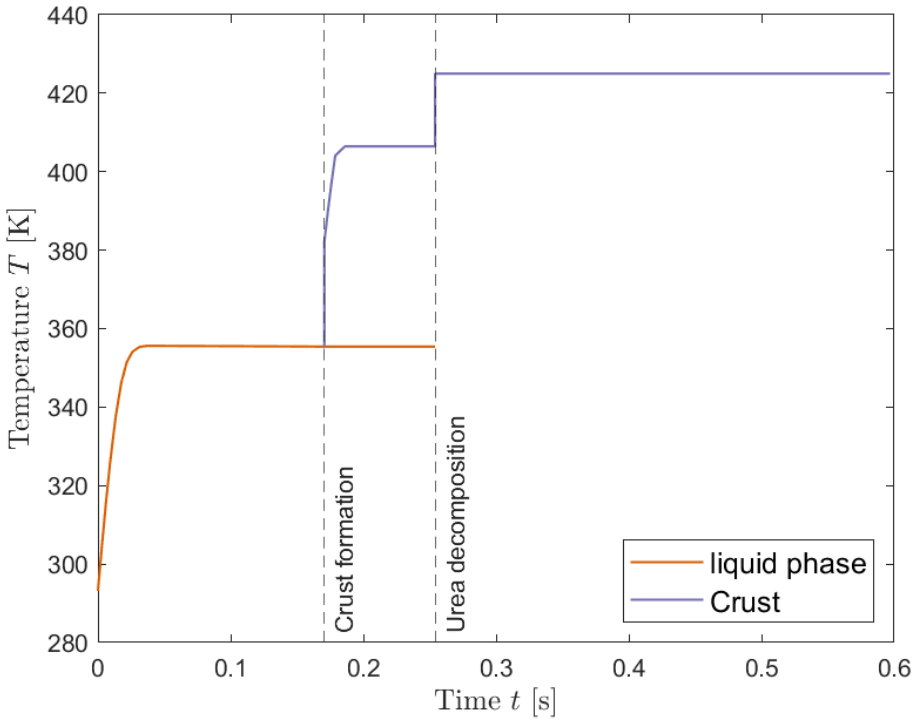

Figure 13: Temperature versus time of the liquid phase and the crust ($r_0 = 200\ \mu m;\ T_\infty = 1223\ K; p_\infty = 1{,}0133\ bar; \xi_{Urea,0} = 0{,}4;\ \left|\frac{d\vec{x}}{dt} - \vec{U}_\infty\right| = 10\frac{m}{s}; \xi_{H2O,\infty} = 0.015;\ \xi_{Urea,\infty} = 0$)

Outlook - Validation with data from SNCR process

To follow up the calculation tool, the urea approach is to implement in the existing model. In addition, the reduction mechanisms DeNOx (NH_3) and RapReNox ($HNCO$) are to be integrated into the calculation following the urea decomposition [10]. Furthermore, the validation of the simplified spray model at a SNCR plant is intend. For this purpose, the model approach must first supplement with the mechanism of NO reduction. Then, by comparing the clean gas NO values and the ammonia slip at the plant with the model results, a simple statement can be made about the validity of the model calculation. The raw gas NO value is required as an important initial value for this purpose. It is the plan to obtain this by briefly shutting down the SNCR.

Summary

This paper presents an optimization concept for an improved additive feed of the SNCR process. First, the potential of an already developed calculation concept has already successfully proven in an application test by comparison with a CFD calculation of a spray process. The advantage in terms of short calculation times is clear. Following on from this, a model approach for the release and thermal decomposition of urea has developed for SNCR operation. For this purpose, three successive release phases are described: The evaporation of pure water, the buildup and drying of a urea crust, and the thermal decay of urea. In parts, the developed calculation methodology could already validated by experimental tests in an ultrasonic levitator.
In a concluding outlook, the further development of the model as well as the planned validation of the intended optimization tool are briefly discussed.

Acknowledgement

At this point, we would like to thank the funding for the AiF-IGF project 20259 BG / 1. Without this funding, the research for this thesis would not have been possible.

References

[1] D. Beerbaum, D. Bernhardt, M. Beckmann, T. Jakobs and T. Kolb, "Entwicklung eines semianalytischen Berechnungswerkzeuges zur Modellierung des Stoffeintrages durch technische Zerstäuber für die Auslegung und Optimierung verfahrenstechnischer Prozesse," in *30. Deutscher Flammentag*, 2021.

[2] K. Srinivasan, T. Sundararajan, S. Narayanan, T. J. S. Jothi and C. S. L. V. R. Sarma, "Acoustic pyrometry in flames," *Measurement,* vol. 46, p. 315–323, January 2013.

[3] R. Koschack and P. Reynolds, "Strahlungspyrometrische Rauchgastemperaturmessung zur SNCR Steuerung an unterschiedlichen Feuerungen und Optimierungspotential für die SNCR," in *Kraftwerkstechnik 2019 - Power plant technology*, Freiberg, 2019.

[4] A. Goanta, M. Strelow, I. Magda, A. Magda and H. Brüggemann, "Development and operating results of U-SNCR technology in coal fired power plants," in *Emissionsminderung in Kraftwerken 2019 - Emission reduction in power plants*, Freiberg, 2019.

[5] B. von der Heide, "Kombination verschiedener SNCR-Technologien zur Einhaltung der neuen EU-Grenzwerte für den NOx-Ausstoß in Kohlekraftwerken," in *Emissionsminderung in Kraftwerken 2019 - Emission reduction in power plants*, Freiberg, 2019.

[6] T. Świeboda, R. Krzyżyńska, A. Bryszewska-Mazurek, W. Mazurek, T. Czapliński and A. Przygoda, "Advanced approach to modeling of pulverized coal boilers for SNCR process optimization - review and recommendations," *International Journal of Thermofluids,* Vols. 7-8, p. 100051, November 2020.

[7] T. D. B. Nguyen, T.-H. Kang, Y.-I. Lim, W.-H. Eom, S.-J. Kim and K.-S. Yoo, "Application of urea-based SNCR to a municipal incinerator: On-site test and CFD simulation," *Chemical Engineering Journal,* vol. 152, p. 36–43, October 2009.

[8] A. David, D. Bernhardt, M. Beckmann, A. Krein and S. Vodegel, "Online-Ermittlung der Abfallzusammensetzung als Basis für eine verbesserte Verbrennungsoptimierung," in *Kraftwerkstechnik 2021 - Power plant technology*, Freiberg, 2021.

[9] S. Ludewig, "Prozessmodellgestützte Optimierung von Primärmaßnahmen zur NOx-Minderung in Rostfeuerungen bei Einsatzstoffen mit unbekannter, zeitlich veränderlicher Zusammensetzung," Papierflieger-Verlag, 2011.

[10] J. A. Miller and C. T. Bowman, "Mechanism and modeling of nitrogen chemistry in combustion," *Progress in Energy and Combustion Science,* vol. 15, p. 287–338, January 1989.

[11] W. Polifke, Wärmeübertragung : Grundlagen, analytische und numerische Methoden, München: Pearson, 2009.

[12] P. Eisenklam, S. A. Arunachalam and J. A. Weston, "Evaporation rates and drag resistance of burning drops," *Symposium (International) on Combustion,* vol. 11, p. 715–728, January 1967.

[13] A. Putnam, "Integratable form of droplet drag coefficient," *J. Am. Rocket Soc.,* vol. 31, p. 1467–1468, 1961.

[14] B. Abramzon and W. A. Sirignano, "Droplet vaporization model for spray combustion calculations," *International Journal of Heat and Mass Transfer,* vol. 32, p. 1605–1618, September 1989.

[15] W. A. Sirignano, Fluid Dynamics and Transport of Droplets and Sprays, Cambridge University Press, 2014.

[16] R. Karpf, "Überblick zur Abgasreinigung," in *10. FachtagungAbgasreinigung vonFeuerungsanlagen und thermische Prozesse*, 2015.

[17] F.-M. Lee and L. E. Lahti, "Solubility of urea in water-alcohol mixtures," *Journal of Chemical and Engineering Data,* vol. 17, p. 304–306, 1972.

[18] C. Yaws, Chemical Properties Handbook: Physical, Thermodynamics, Environmental Transport, Safety & Health Related Properties for Organic &, MCGRAW HILL BOOK CO, 1998.

[19] M. Koebel, M. Elsener and M. Kleemann, "Urea-SCR: a promising technique to reduce NOx emissions from automotive diesel engines," *Catalysis Today,* vol. 59, p. 335–345, June 2000.

[20] A. Lundström, B. Waldheim, H. Ström and B. Westerberg, "Modelling of urea gas phase thermolysis and theoretical details on urea evaporation," *Proceedings of the Institution of*

Mechanical Engineers, Part D: Journal of Automobile Engineering, vol. 225, p. 1392–1398, July 2011.

[21] A. M. Bernhard, I. Czekaj, M. Elsener, A. Wokaun and O. Kröcher, "Evaporation of Urea at Atmospheric Pressure," *The Journal of Physical Chemistry A,* vol. 115, p. 2581–2589, March 2011.

[22] P. M. Schaber, J. Colson, S. Higgins, D. Thielen, B. Anspach and J. Brauer, "Thermal decomposition (pyrolysis) of urea in an open reaction vessel," *Thermochimica Acta,* vol. 424, p. 131–142, December 2004.

[23] G. L. Hubbard, V. E. Denny and A. F. Mills, "Droplet evaporation: Effects of transients and variable properties," *International Journal of Heat and Mass Transfer,* vol. 18, p. 1003–1008, September 1975.

[24] M. Mezhericher, A. Levy and I. Borde, "Theoretical Drying Model of Single Droplets Containing Insoluble or Dissolved Solids," *Drying Technology,* vol. 25, p. 1025–1032, June 2007.

[25] N. Abuaf and F. W. Staub, "Drying of liquid-solid slurry droplets," General Electric, Corporate Research and Development, 1985.

[26] H. Ström, A. Lundström and B. Andersson, "Choice of urea-spray models in CFD simulations of urea-SCR systems," *Chemical Engineering Journal,* vol. 150, p. 69–82, July 2009.

[27] N. Frössling, "On the evaporation of falling drops," *Gerl. Beitr. Zur Geophysik,* p. 170–216, 1938.

[28] D. R. Lide and W. M. ". Haynes, Eds., CRC handbook of chemistry and physics, 90th ed., CRC Press, 2010.

[29] H.-J. Kretzschmar, *KCE-ThermoFluidProperties UG & Co. KG - FluidLAB,* 2022.

Symbols and indices

Table 1: Symbols

a	Thermal diffusivity	$\left[\frac{m^2}{s}\right]$
B_M	Spalding Number	$[-]$
c	Specific heat capacity	$\left[\frac{J}{kgK}\right]$
CN_3H_4O	Urea	
D	Diffusivity	$\left[\frac{m^2}{s}\right]$
$\vec{F}$	Force	$[N]$
h	Specific enthalpy	$\left[\frac{J}{kg}\right]$
$HNCO$	Isocyanic acid	
m	Mass	$[kg]$
NH_3	Ammonia	$[-]$
Nu	Nusselt number	$[-]$
NO	Nitrogen oxides (nitrogen monoxide)	$[-]$
p	Pressure	[Pa]
Pr	Prandtl number	$[-]$
r	Radius	$[m]$
R	Specific gas constant	$\left[\frac{J}{kg \cdot K}\right]$

Re	Reynolds number	$[-]$
t	Time	$[s]$
T	Absolute temperature	$[K]$
$\vec{U}$	Velocity	$\left[\frac{m}{s}\right]$
$\dot{V}$	Volume flow	$\left[\frac{\mathrm{m}^3}{\mathrm{s}}\right]$
$\vec{x}$	Location	$[m]$
Δh	Enthalpy change	$\left[\frac{J}{kg}\right]$
ε	Porosity	$[-]$
λ	Heat conductivity	$\left[\frac{W}{m \cdot K}\right]$
ξ	Mass fraction	$[-]$
ϑ	Temperature	$[°C]$
ρ	Density	$\left[\frac{kg}{m^3}\right]$

Table 2: Indices

CS	Crust surface
WS	Wet surface
D	Droplet
$decomp$	Decomposition
ev	Evaporation
$film$	Film composition
$H2O$	Water
HP	Heat Cartridge
l	Liquid
p	Constant pressure (isobar)
S	Surface
v	Vapour
0	Initial
∞	Ambient